Immunity 25, 117–127, July 2006 ©2006 Elsevier Inc. DOI 10.1016/j.immuni.2006.04.010

T Cell Receptor-Proximal Signals Are Sustained in Peripheral Microclusters and Terminated in the Central Supramolecular Activation Cluster

Rajat Varma,[1] Gabriele Campi,[1] Tadashi Yokosuka,[2] Takashi Saito,[2] and Michael L. Dustin[1,*]
[1] Program in Molecular Pathogenesis
Skirball Institute of Biomolecular Medicine
Department of Pathology
New York University School of Medicine
540 First Avenue
New York, New York 10016
[2] Laboratory for Cell Signaling
RIKEN Center for Allergy and Immunology (RCAI)
1-7-22, Suehiro-cho, Tsurumi-ku
Yokohama 230-0045
Japan

Summary

T cell receptor (TCR) signaling is initiated and sustained in microclusters; however, it's not known whether signaling also occurs in the TCR-rich central supramolecular activation cluster (cSMAC). We showed that the cSMAC formed by fusion of microclusters contained more CD45 than microclusters and is a site enriched in lysobisphosphatidic acid, a lipid involved in sorting ubiquitinated membrane proteins for degradation. Calcium signaling via TCR was blocked within 2 min by anti-MHCp treatment and 1 min by latrunculin-A treatment. TCR-MHCp interactions in the cSMAC survived these perturbations for 10 min and hence were not sufficient to sustain signaling. TCR microclusters were also resistant to disruption by anti-MHCp and latrunculin-A treatments. We propose that TCR signaling is sustained by stabilized microclusters and is terminated in the cSMAC, a structure from which TCR are sorted for degradation. Our studies reveal a role for F-actin in TCR signaling beyond microcluster formation.

Introduction

Sensitive T cell activation requires the cooperation of T cell receptors (TCRs) and adhesion molecules because the TCRs and MHC-peptide complexes (MHCp) are small membrane-associated proteins that interact with low affinity and relevant MHCp are present in low abundance (Shaw and Dustin, 1997; Shimizu et al., 1990; Springer, 1990). A widely studied paradigm is based on the utilization of lymphocyte function antigen-1 (LFA-1) on T cells and intercellular adhesion molecule-1 (ICAM-1) on antigen-presenting cells as a major adhesion and costimulation system leading to a highly compartmentalized interface (Monks et al., 1998). This LFA-1-based immunological synapse (IS) is composed of a central cluster of TCR-MHCp interactions known as the central supramolecular activation cluster (cSMAC) surrounded by a ring of LFA-1-ICAM-1 interactions known as the peripheral SMAC (pSMAC) (Bromley et al., 2001; Monks et al., 1998) and an outer fringe of membrane enriched in CD45 known as the distal SMAC (dSMAC) (Freiberg et al., 2002). TCR microclusters have been observed early in T cell-APC interactions that converge to form the cSMAC (Krummel et al., 2000). Some T cell-DC IS are composed entirely of TCR microclusters (Brossard et al., 2005).

The cSMAC has been proposed to represent a site of sustained signaling based upon the central concentration of the tyrosine kinase Lck (Ehrlich et al., 2002; Monks et al., 1998), phosphatidylinositol-3-kinase products (Costello et al., 2002; Huppa et al., 2003), and self-MHCp that participate in signaling (Irvine et al., 2002; Krogsgaard et al., 2005). The cSMAC is also a site where TCR and CD45 interact to reset signaling, a transient decrease in signaling needed for sustained signaling (Freiberg et al., 2002). It has been proposed that the cSMAC contributes to TCR degradation (Lee et al., 2002, 2003). TCR degradation takes place via ubiquitination and targeting to multivesicular bodies that are enriched in lysobisphosphatidic acid (LBPA) in the lysosomal pathway (Liu et al., 2000; Matsuo et al., 2004). Whether the cSMAC directly participates in the process of multivesicular body formation based on accumulation of markers such as LBPA has not been demonstrated.

ICAM-1 and agonist MHCp complexes in a supported planar bilayer trigger TCR clustering and are laterally mobile such that an IS with SMACs forms and fully activates T cells (Dustin and Colman, 2002; Grakoui et al., 1999). In this system, the cSMAC is a site of stable TCR-MHCp interactions (Grakoui et al., 1999). Recently, total internal reflection fluorescence microscopy has been used with this system to demonstrate continuous formation of TCR microclusters that sustain TCR signaling (Campi et al., 2005; Yokosuka et al., 2005). The initial size of TCR microclusters is proportional to the density of agonist MHCp in the planar bilayer (Yokosuka et al., 2005). After the cSMAC forms, the microclusters continue to form and are sites of TCR signaling based on recruitment of phosphorylated Lck, ZAP-70, and LAT and the adaptor protein SLP-76 (Campi et al., 2005; Yokosuka et al., 2005). Due to the transport process, each peripheral microcluster lasts only about 2 min before merging with the cSMAC. Physically holding TCR microclusters in the periphery augments signaling (Mossman et al., 2005). These findings suggest that peripheral TCR microclusters are important signaling structures but do not address the signaling capability of the cSMAC.

TCR-MHCp interactions are required to sustain T cell signaling over a period of hours to fully activate $CD4^+$ T cells (Beeson et al., 1996; Costello et al., 2002; Hashemi et al., 1996; Huppa et al., 2003; Iezzi et al., 1998; Lee et al., 2002). MHCp antibodies reduce Ca^{2+} to baseline by 15 min (Huppa et al., 2003). Multivalent TCR-MHCp interactions are relatively resistant to dissociation by inhibitory antibodies as demonstrated by tetramer dissociation (Savage and Davis, 2001). For example, I-E^k-moth cytochrome C (MCC) 88-103 tetramers dissociate from T cells expressing the 2B4 TCR with a half-life of

*Correspondence: dustin@saturn.med.nyu.edu

1 hr (Malherbe et al., 2004), while the intrinsic half-time for binding is 36 s (Krogsgaard et al., 2003). The avidity of TCR-MHCp interactions in microclusters and the cSMAC are not known.

How microclusters and the cSMAC differ in composition and signaling potential are important open questions. In this report, we defined the time at which individual TCR clusters link together to form the cSMAC, determined the relationship of CD45 to microclusters and the cSMAC, determined whether LBPA is recruited to microclusters or the cSMAC, determined the stability of TCR-MHCp interactions in microclusters and the cSMAC, and exploited differences in the lifetime of microclusters and the cSMAC to define their roles in calcium signaling. We conclude that stable TCR microclusters exclude CD45 and contribute to calcium signaling. In contrast, the cSMAC does not exclude CD45 as effectively, marking its loss of signaling competence, and is rich in LBPA, marking its potential to directly participate in TCR elimination.

Results

TCR Microclusters Join to Form the cSMAC

Signaling is initiated and sustained in TCR microclusters that are formed continuously in the periphery of the IS and transported to the center to form the cSMAC (Campi et al., 2005; Yokosuka et al., 2005). We first asked whether the cSMAC remains a collection of independent microclusters or if they interact in a specific manner to form a unique integrated structure. To answer this question, we employed TIRFM to follow TCR labeled with Alexa-(488 or 568) H57 Fab on in vitro activated AND TCR Transgenic (Tg) T cells interacting with supported planar bilayers containing glycosyl-phosphatidylinositol (GPI) anchored forms of I-E^k (GPI-I-E^k) loaded with an agonist peptide derived from moth cytochrome C (MCC88-103) (agonist MHCp, 10 molecules/μm^2) and GPI-ICAM-1 (300 molecules/μm^2). TCR clusters formed rapidly, as indicated by clustering of TCR labeled with H57 Fab and direct visualization of fluorescent MHCp in the bilayer (Figures S1A–S1C in the Supplemental Data available with this article online) and translocated to the center of the IS (Figures 1A–1E and Movie S1), consistent with recent descriptions of peripheral TCR microclusters (Campi et al., 2005; Yokosuka et al., 2005). Initially, the microclusters moved independently of each other, but within 5 min microclusters fuse to form larger clusters that continue to show relative "jostling" movements, represented by colored areas in Figures 1F–1I, and become immobilized in an interconnected network between 5 and 15 min (Figures 1H and 1I). We defined these events, taking place between 5 and 15 min, as cSMAC formation.

Sustained TCR Microclusters Have a Narrow Range of Sizes

We next used TIRFM to estimate the number of TCRs in microclusters under conditions of sustained signaling (>30 min). TCR were labeled with Alexa-568 H57 Fab as described above. TCR clustering in microclusters and the cSMAC was not due to membrane accumulation of vesicles based on double staining experiments with the membrane dye DiI and experiments with control Fab (Figures S1D–S1J). Calibration of TIRFM is challenging due to the sensitivity of the illumination to small changes in the angle of the laser beam, but our system was stable enough to allow collection of an entire data set covering a range from 0 to 20 MHCp/μm^2 without adjustment. We used the TCR signal of 25 cells adhering to ICAM-1 containing bilayers to determine the average fluorescence signal representing the average resting density of TCR, which was 140 molecules/μm^2 (Campi et al., 2005), and then we used this calibration factor for all measurements. Interestingly, the TCR distribution was not uniform on cells adhering to GPI-ICAM-1, and distinct clusters with an average of 6.7 TCR each were detected (Figures S2A and S2F). This number was consistent with recent reports of preclustering of TCR (Schamel et al., 2005). As previously reported, the cSMAC size was linearly related to the initial density of agonist MHCp in the bilayer between 0.2 and 20 molecules/μm^2 of GPI-I-E^k-MCC88-103 (Grakoui et al., 1999), the range over which sustained Ca^{2+} signaling was observed (Figure S2G). By 30 min, the microclusters had decreased in size to between 11 TCR at 0.2 MHCp/μm^2 and 17 TCR at 20 MHCp/μm^2 (Figures S2B, S2C, and S2F). Thus, a more than 100-fold range of MHCp densities the TCR microcluster size converges to a 2-fold size range. This suggests that a minimum size TCR microcluster may be needed to sustain signaling.

Microclusters Exclude CD45

CD45 is excluded from sites of active TCR signaling (Bunnell et al., 2002; Choudhuri et al., 2005), but variable results have been obtained for CD45 in the cSMAC (Johnson et al., 2000; Leupin et al., 2000; Sperling et al., 1998; Zaru et al., 2002). We reinvestigated CD45 localization by TIRFM. We bound Alexa488-I3/2.3 Fab and Alexa568-H57 Fab to AND TCR Tg T cells and imaged the interaction with bilayers containing 10 molecules/μm^2 GPI-I-E^k-MCC88-103 and GPI-ICAM-1 by TIRFM. We found that CD45 was excluded from all early TCR microclusters (Figures 1J–1L), which had an average diameter of 0.52 ± 0.056 μm (n = 4, total of 180 microclusters measured). After cSMAC formation, CD45 was still excluded from peripheral microclusters, although this was less visible in smaller clusters (Figures 1M–1O), but CD45 was included in 93% of cSMACs (see inset, Figures 1M–1O). Quantifying fluorophore exclusion from submicron diameter areas is complicated by the spill over of signal into the exclusion zone from surrounding fluorophores. A point spread function is the intensity distribution measured from a point source of light, for example a fluorescent subresolution bead, and is a measure of the resolution of the microscope. We used an experimental point spread function for our TIRFM microscope to simulate the image that would be obtained with an object having 100% exclusion of fluorophores from a 0.55 μm diameter region surrounded by uniform fluorescence. The simulated image is quantitatively similar to images of CD45 exclusion from similar sized TCR microclusters at 30 s and 15 min (Figure S3). Inclusion of TCR with CD45 in the core of the cSMAC is consistent with FRET data in a cell-cell system showing close proximity of TCR and CD45 in the cSMAC but not in the periphery (Freiberg et al., 2002).

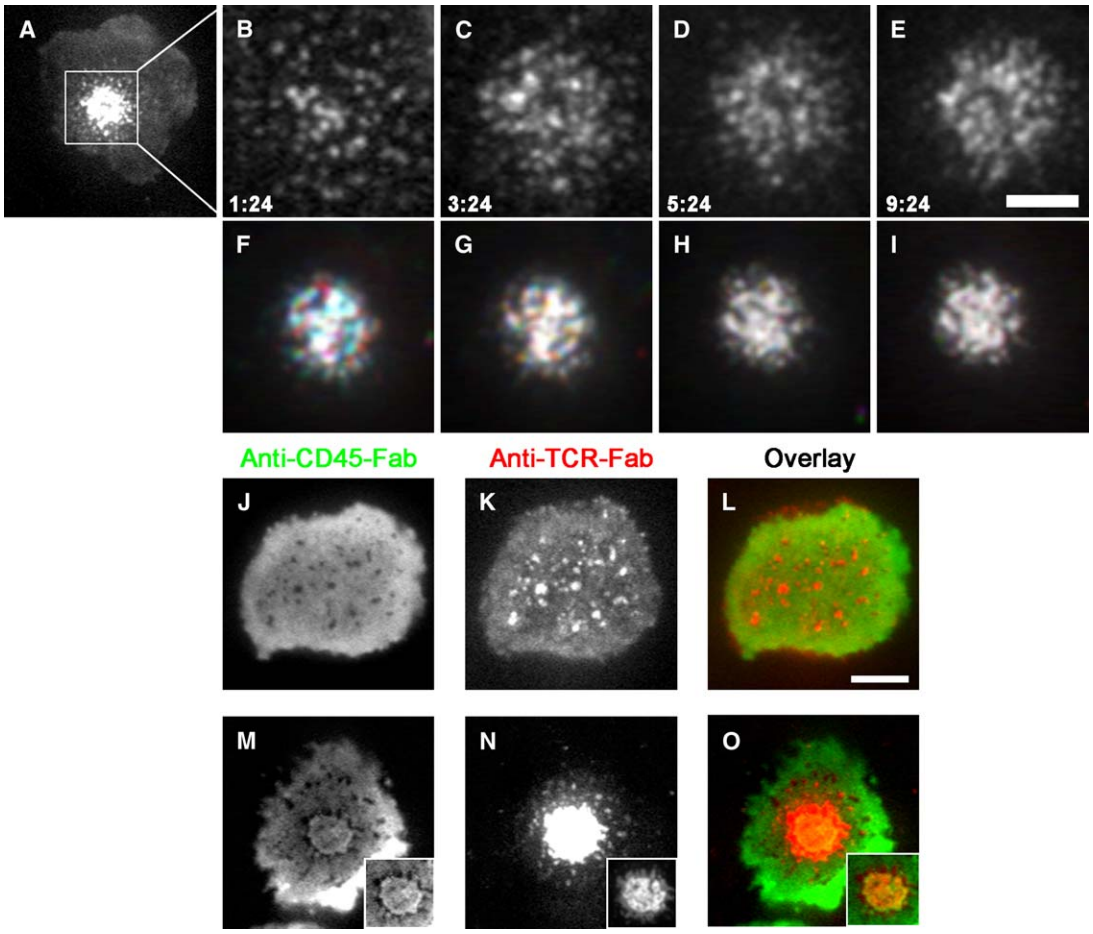

Figure 1. cSMAC Formation and CD45 Exclusion from Microclusters

(A–E) TCRs were visualized by TIRFM of Alexa-488-H57-Fab-labeled AND T cells forming IS on glass-supported bilayers containing ICAM-1 and 10 agonist MHCp/μm^2. (B)–(E) represent TIRFM images of the box around the cSMAC in (A). The cSMAC region starts out as a collection of microclusters (B), and these microclusters fuse to form the cSMAC structure. Images in (B) and (C) were scaled relative to (D) and (E) for visualization of microclusters.

(F–I) Each image in these panels represent three sequential frames in a time course observing cSMAC formation color coded in red, green, and blue and overlayed that are 6 s apart. Structures that appear white are those that are not undergoing motion, while portions that appear colored are those that are undergoing substantial motion. 5–6 min after contact formation (F and G), there is more relative motion among clusters than at 10–12 min (H and I). Scale bar in (E) equals 2 μm. Similar data were obtained from at least four independent experiments.

(J–O) CD45 and TCR were visualized by TIRFM of Alexa-488-I3/2.3-Fab and Alexa-568-H57-Fab-labeled AND T cells forming IS on glass-supported bilayers containing ICAM-1 and 10 agonist MHCp/μm^2. (J–L) Representative images of cells forming TCR microclusters (K) 30 s post contact formation that exclude CD45. (M–O) Representative images of cells 30 min post synapse formation. Microclusters formed at 30 min (N) continue to exclude CD45 (M); however, 93% of the cSMACs (see insets) are now enriched in CD45 (three independent experiments, total n = 45 cSMACs measured). Scale bar in (L) equals 4 μm.

LBPA Is Accumulated in the cSMAC, but Not Microclusters

The cSMAC has been proposed as a site for TCR degradation. LBPA is a lipid that is generated at the site of multivesicular body formation—a process necessary for sorting of membrane proteins for degradation (Kobayashi et al., 1999; Matsuo et al., 2004; Mobius et al., 2003). We examined the distribution of LBPA in the IS of detergent-permeabilized cells by TIRFM immunofluorescence analysis with LBPA monoclonal antibody (Figured 2A–2L) and compared it to an isotype control antibody (Figures 2M–2P; Kobayashi et al., 1999). There was no specific staining for LBPA associated with T cells adhering to planar bilayers containing ICAM-1 by TIRFM (Figures 2I–2L) or wide-field microscopy (data not shown). When Alexa-568 H57-labeled AND TCR Tg T cells interacted with planar bilayers containing 2 (Figures 2A–2D) or 10 (Figures 2E–2H) GPI-I-E^k-MCC88-103 and GPI-ICAM-1, the accumulation of LBPA in or near the cSMAC of the fixed cells was observed in 60% of the IS. Wide-field imaging revealed that LBPA was also present in cytoplasmic structures proximal to the cSMAC (data not shown). No LBPA was associated with TCR microclusters (Figure S4). The presence of LBPA in proximity of the cSMAC is consistent with it being a degradative compartment.

Anti-MHCp and F-Actin Depolymerization Block Sustained Ca^{2+} Signaling

To understand the site for sustained signaling in the IS, we decided to use two perturbations that are known to acutely block ongoing Ca^{2+} signaling in T cells. We

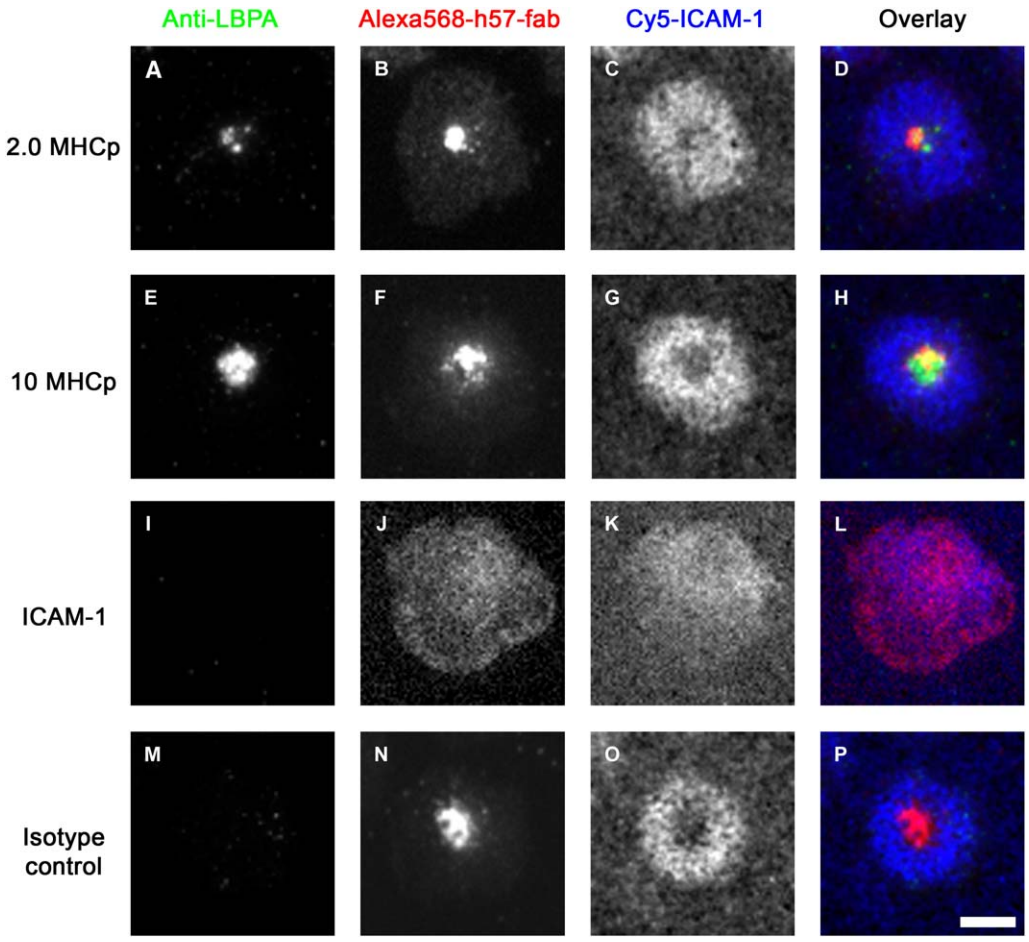

Figure 2. Localization of LBPA in the IS

AND T cells interacting with bilayers containing the indicated amounts of agonist-MHCp were fixed at 20 min and stained for TCR and LBPA. Enrichment of LBPA in the cSMAC is observed at 2.0 (A–D) and 10.0 agonist (E–H) MHCp/μm^2. AND T cells interacting with bilayers containing ICAM-1 did not show any staining in the TIRF field (I–L). The specificity of the antibody was determined with a isotype control antibody (M–P). Similar results were obtained from at least three independent experiments. Scale bar equals 4 μm.

used a mixture of 14-4-4 (anti-I-E^k) and D4 (anti-I-E^k in complex with MCC88-103) (30 μg/ml each) (Reay et al., 2000) to block TCR-MHCp interactions and latrunculin-A to depolymerize the F-actin cytoskeleton. Although it is well established that these treatments inhibit Ca^{2+} signaling downstream of the TCR (Huppa et al., 2003; Valitutti et al., 1995), we needed to determine the precise time course of inhibition in order to relate the time scale of signaling changes to the time scale of changes in TCR-MHCp interactions in the cSMAC and microclusters. We used Fura-2 ratio imaging to follow the changes in cytoplasmic Ca^{2+}. AND TCR Tg T cells that had interacted with bilayers containing GPI-I-E^k-MCC88-103 and GPI-ICAM-1 for 30 min were treated with the D4 and 14-4-4 mix. D4 and 14-4-4 treatment reduced Ca^{2+} to baseline within 2 min (Figures 3A and 3B), whereas latrunculin-A treatment reduced Ca^{2+} to baseline in less than 1 min (Figures 3C and 3D). Cells that were not subject to either treatment sustained cytoplasmic calcium over the relevant time periods (Figure S5). By knowing the time scales associated with signal elimination by these perturbations, we could now interpret experiments examining the response of the cSMAC and microcluster to the same perturbations.

The cSMAC and Microclusters Resist Disruption by Anti-MHCp

We next tested the fate of TCR-MHCp interactions within the cSMAC and microclusters to disruption with MHCp antibodies. We treated IS-forming AND T cells with a mixture of 14-4-4 and D4 antibodies 20–30 min after IS formation. We evaluated the avidity of interactions in the cSMAC by determining the number of labeled MHCp remaining in the cSMAC and the stability of the H57 Fab-labeled TCR remaining in the cSMAC after anti-MHCp treatment. Over a period of 10 min after D4 and 14-4-4 treatment, the pSMAC became disorganized, but 80% of MHCp (Figures 4A–4C) and TCR (Figures 4D–4F) in the cSMAC were retained. Parallel experiments with fluorescent H57 IgG demonstrated saturation staining of the cSMAC in 3 min (Figure S6). Therefore, the failure of the anti-MHCp mixture to rapidly reverse the cSMAC is likely due to a high probability of rebinding of TCR to MHCp after each spontaneous dissociation event. Antibodies enter the $\geq$15 nm space between the T cell and planar bilayers (Figure S6), but will likely be excluded from the $\leq$1 nm space in the TCR-MHCp encounter complex. Rapid rebinding of MHCp to TCR without intervening escape of MHCp from the

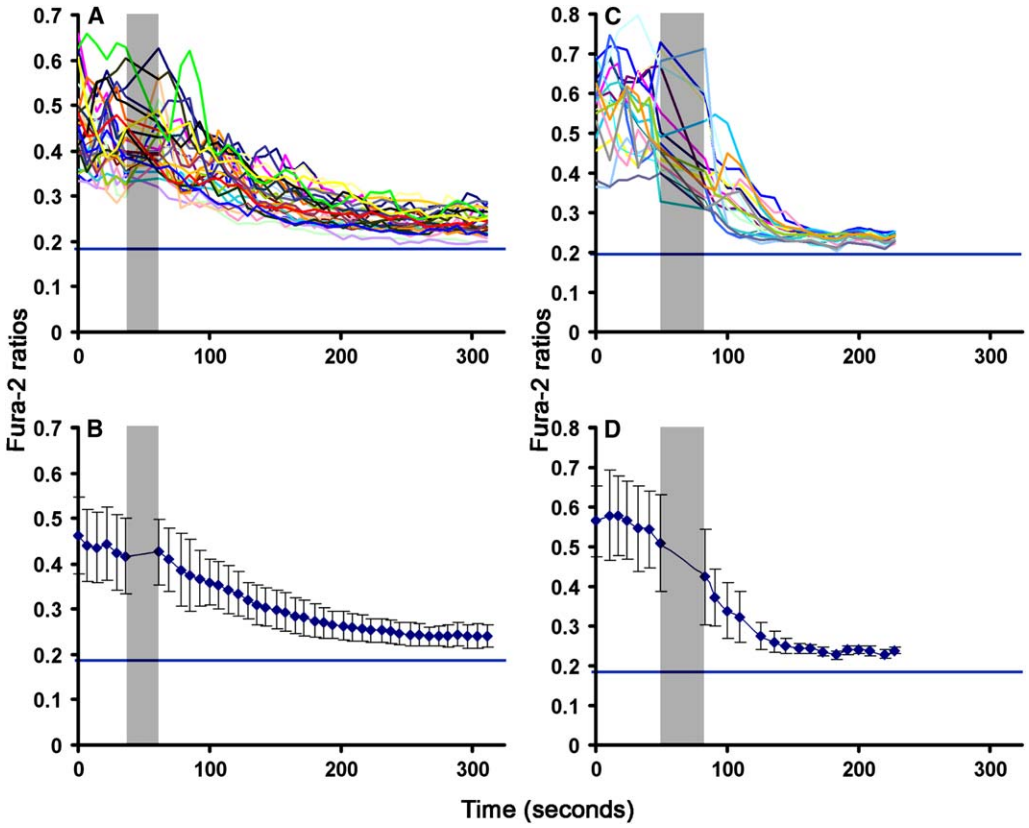

Figure 3. MHCp Antibodies and Latrunculin-A Inhibit Sustained Calcium Signaling in T Cells Forming IS

AND TCR Tg T cells were labeled with Fura-2-AM and were incubated with supported planar bilayers containing ICAM-1 and 10 agonist MHCp/μm^2. 25 min after IS formation, the 340/380 ratio was determined by wide-field fluorescence microscopy every 5 s. The low and high calcium ratios corresponding to cells in EGTA Mg^{2+} (+) Ca^{2+} (−) buffer and ionomycin were also determined. Injections of anti-MHCp (A and B) or latrunculin-A (C and D) are indicated as dark gray bar in graphs. Individual cell values (A and C) and population averages (B and D) show that cytoplasmic Ca^{2+} concentration reduced in 2 min after anti-MHCp treatment and 1 min after latrunculin-A treatment. The blue line in each graph represents calcium concentration of cells treated with EGTA Mg^{2+} (+) Ca^{2+} (−) buffer. Error bars in (B) and (D) represent standard deviation. Similar results were obtained from two independent experiments.

encounter complex is a form of "avidity" leading to stability of the TCR microclusters. After D4 and 14-4-4 treatment, the peripheral microclusters completed their transit to the cSMAC over a period of 2 min (Figures 4G–4J), but no new microclusters formed (Figures 4I and 4J). Movie S2 shows the effect of MHCp antibodies on the dynamics of H57 Fab-labeled TCR. The formation of new TCR microclusters was unaffected by a control mouse IgG. Thus, microclusters and cSMACs displayed high stability in the presence of MHCp antibodies. These results suggest that calcium signaling is not sustained by interactions in the cSMAC but require the continuous formation of TCR microclusters in the periphery.

Anti-MHCp Inhibition of New Microclusters Stops Zap-70 Recruitment

The recruitment of Zap-70-GFP to TCR microclusters correlates with sustained signaling (Yokosuka et al., 2005). Zap-70-GFP was introduced into AND TCR Tg T cells by retroviral transduction, and the cells were allowed to form IS on bilayers containing agonist MHCp and ICAM-1. After 30 min, the movement of Zap-70-GFP-positive clusters from the pSMAC to the cSMAC was evaluated by confocal microscopy before and after addition of D4 and 14-4-4 antibody mix. As previously described, Zap-70-GFP accumulated in discrete clusters that translocated at ~2 μm/min and fade as they reach the cSMAC (Figures 4K and 4L, Movie S3; Yokosuka et al., 2005). After D4 and 14-4-4 treatment, the already formed Zap-70-GFP clusters continued to move to the cSMAC and fade as they reached the cSMAC (Figures 4M and 4N, Movie S3). D4 and 14-4-4 treatment immediately eliminated formation of new Zap-70-GFP microclusters. The time required for microclusters to reach the cSMAC corresponds closely with the time required to extinguish signaling after D4 and 14-4-4 treatment. Zap-70-GFP associated with the cSMAC did not change after D4 and 14-4-4 treatment. This suggests that cSMAC-associated Zap-70 was nonfunctional in signaling for Ca^{2+} elevation.

The cSMAC Is F-Actin Independent

TCR microcluster formation by AND TCR Tg T cells on bilayers with agonist MHCp and ICAM-1 is dependent upon F-actin (Campi et al., 2005). In order to understand how F-actin contributes to the maintenance of microclusters, we tested the effect of latrunculin-A on IS undergoing sustained signaling at 30 min. We measured cSMAC avidity by quantifying the number of fluorescent MHCp complexes retained in the cSMAC

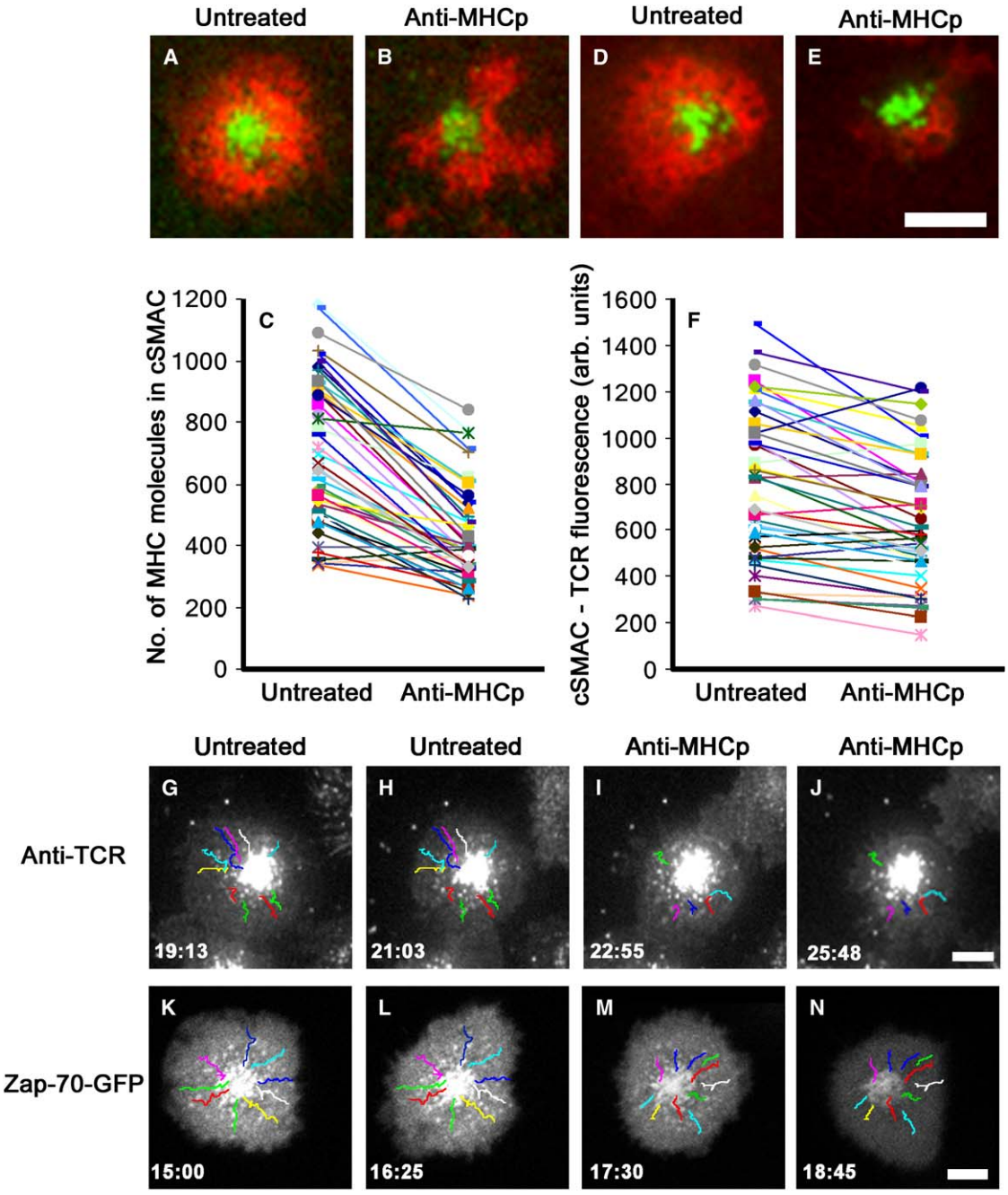

Figure 4. MHCp Antibody Treatment Does Not Disrupt the cSMAC or Microclusters, but Prevents New Microcluster Formation

Images of AND T cell forming an IS on bilayers containing ICAM-1 and 10 agonist MHCp/μm^2 before (A, D) and after (B, E) treating cells with MHCp antibodies (red; Cy5-Icam-1, green; Oregon Green I-E^K in [A] and [B] and Alexa-488-H57-Fab in [D] and [E]). Scale bar equals 4 μm. TCR-MHCp interactions in the cSMAC are at 80% of initial levels at 10 min after addition of anti-MHCp antibodies based on retention of I-E^k fluorescence (C) and TCR fluorescence (F). A line connects data points for each cell before and after treatment. Some cells have no reduction in TCR-MHCp interaction, yet all cells show reduced Ca^{2+}. Microclusters continue to form up to 30–60 min in the mature IS (G, H). Treatment with anti-MHCp blocked formation of new microclusters; however, the existing microclusters were chased into the cSMAC (I, J). Zap-70-GFP was introduced into AND T cells via retroviral transduction. Confocal imaging was performed on these cells interacting with bilayers containing ICAM-1 and 10 agonist MHCp/μm^2. Microclusters recruit Zap-70 and fade as they approach the cSMAC (K, L). Treatment with anti-MHCp blocked the recruitment of Zap-70 to the microclusters, and the existing ones were chased into the cSMAC by 1–2 min. Tracks shown start in frames (G), (I), (K), and (M) and end in frames (H), (J), (L), and (N). Similar results were obtained from three independent experiments. Scale bar equals 4 μm.

(Figures 5A–5C), and we measured TCR stability by quantifying the relative TCR fluorescence associated with the cSMAC (Figures 5D–5F). Latrunculin-A treatment caused disorganization of the pSMAC (Figures 5B and 5E, red), but only small changes in the cSMAC (Figures 5B and 5E, green). The cSMACs were resistant to disruption by latrunculin-A based on retention of 80% of MHCp and TCR signals in the cSMAC at 10 min after treatment (Figures 5C and 5F). We next examined the effect of latrunculin-A on microclusters by

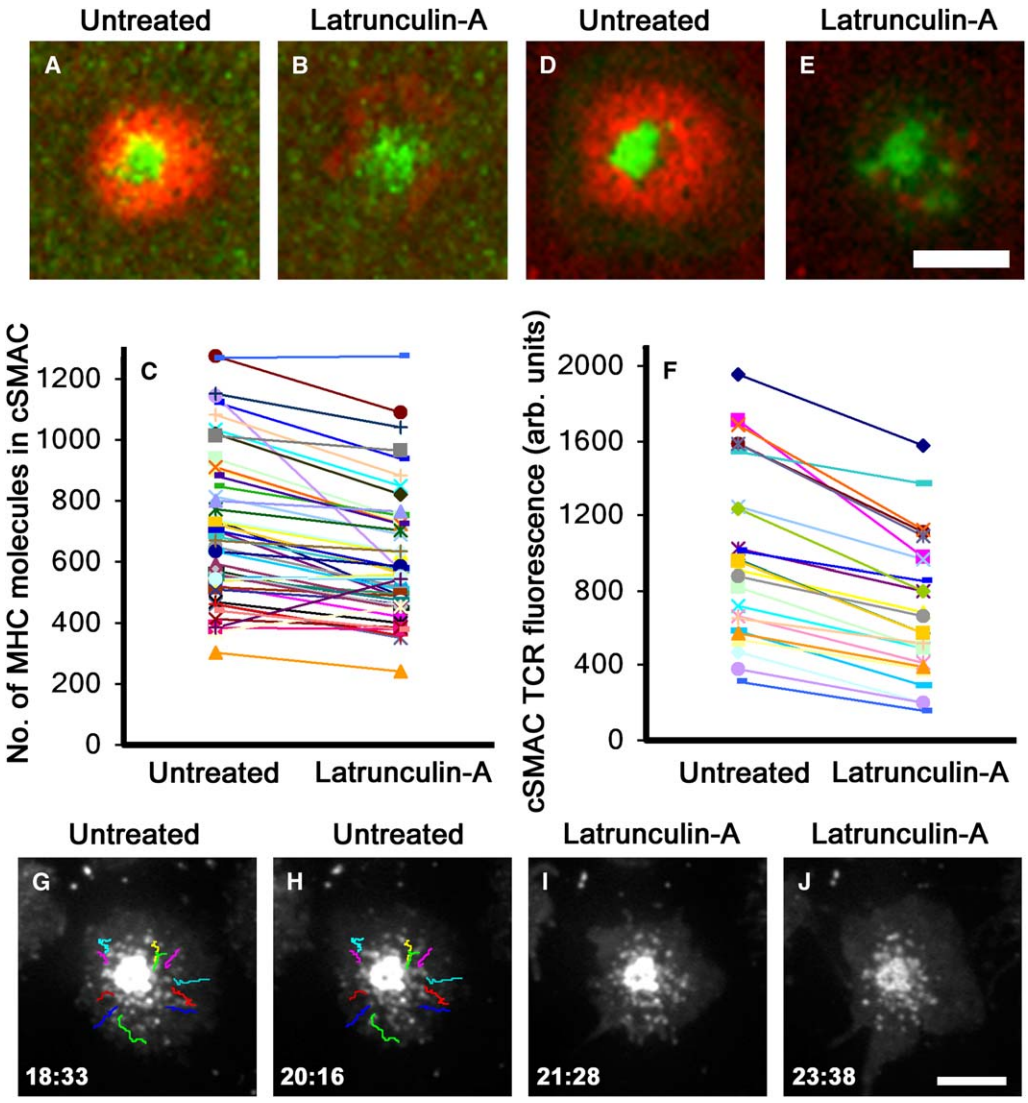

Figure 5. F-Actin Depolymerization Arrests Microclusters but Does Not Disrupt Microclusters or the cSMAC

Images of AND T cell forming an IS on bilayers containing ICAM-1 and 10 agonist MHCp/μm^2 before (A, D) and after (B, E) treating cells with latrunculin-A (red; Cy5-Icam-1, green; Oregon Green I-E^k in [A] and [B] and Alexa-488-H57-Fab in [D] and [E]). Scale bar equals 4 μm. TCR-MHCp interactions in the cSMAC are at 80% of initial levels at 10 min after addition of latrunculin-A based on retention of I-E^k fluorescence (C) and TCR fluorescence (F). A line connects data points for each cell before and after treatment. The translocation of microclusters toward the cSMAC in the mature IS was imaged with TIRFM and tracked at 30 min (G–J). Latrunculin-A prevented the formation of new microclusters and many microclusters in the periphery were dispersed, while some near the cSMAC persisted and their translocation was blocked. Similar results were obtained from two independent experiments. Scale bar equals 4 μm.

TIRFM (Figures 5G–5J and Movie S4). Microclusters stopped translocating immediately after latrunculin-A treatment. Many of the arrested microclusters persisted for many minutes, particularly those closer to the cSMAC. As expected, no new microclusters formed after latrunculin-A treatment (Movie S4). Thus, the stability of the cSMAC does not depend on actin.

TCR Microclusters Are High-Stability Structures

The result that microclusters have a high stability independent of F-actin has important implications for T cell sensitivity, so we wanted to determine if this property was manifested before cSMAC formation. We added D4 and 14-4-4 to T cells that were undergoing the expansion phase of IS formation and had just formed an array of TCR microclusters after 30 s. Treatment with D4 and 14-4-4 at this stage arrested TCR microclusters without cSMAC formation (Movie S5). The microclusters were stable for ~6 min (Figures 6A–6E), after which the cells began to migrate and shed the TCR clusters. The stability of TCR microclusters was F-actin independent, as shown by the observation that treatment with latrunculin-A at 30 s arrested newly formed microclusters but did not disrupt the TCR clusters for at least 5 min (Figures 6F–6J, Movie S6). Latrunculin-A eliminates F-actin from previously actin-positive peripheral microclusters within 1 min, the time frame for loss of Ca^{2+} signaling (Figure S7). Thus, microcluster

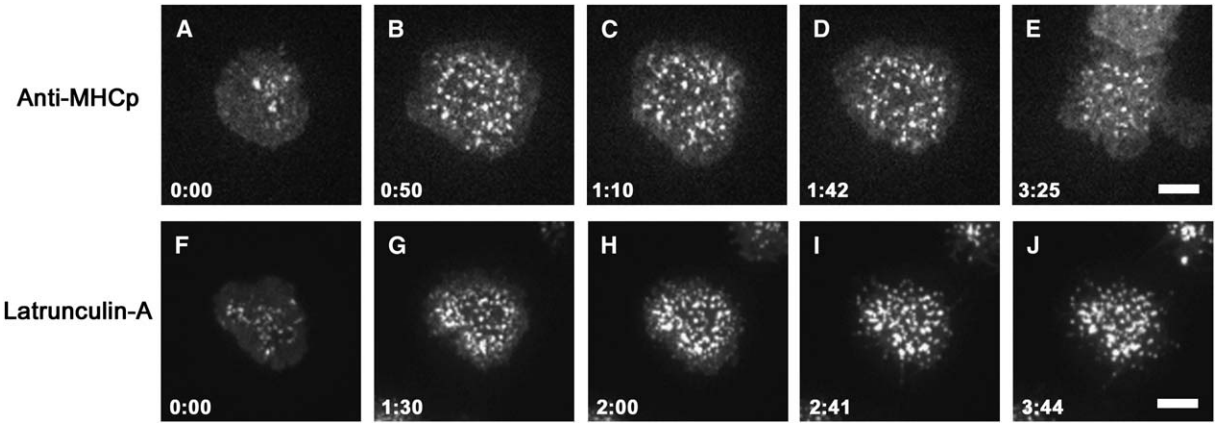

Figure 6. Microclusters Are High-Avidity Structures Based on Resistance to Anti-MHCp and Latrunculin-A

TCRs were visualized by TIRFM of Alexa-488-H57-Fab-labeled AND T cells forming IS on glass-supported bilayers containing ICAM-1 and 10 agonist MHCp/μm^2. Cells were treated with anti-MHCp (A–E) or latrunculin-A (F–J) when they formed an immature synapse or were in the expansion phase. Anti-MHCp was added between (B) and (C) and latrunculin-A was added between (G) and (H). Microclusters showed resistance to both these treatments, as shown in (C)–(E) and (H)–(J). Similar results were obtained from two independent experiments. Scale bar equals 4 μm.

formation is F-actin dependent as previously shown (Campi et al., 2005), but the microclusters rapidly become F-actin independent for stability but not signaling.

Discussion

Our data supports a model in which there are three distinct types of TCR clusters in the IS. On a nonadherent cell surface, we assume that TCR and LFA-1 are uniformly distributed. Upon adhesion, we have observed formation of small TCR clusters. We would speculate that integrin-mediated remodeling of the cortical actin cytoskeleton is responsible for this antigen-independent TCR clustering. Although we provide no evidence that these clusters function to enhance formation of signaling microclusters, support for this hypothesis has been shown (Schamel et al., 2005). Upon engagement by MHCp, F-actin-dependent TCR microclusters with a high stability are formed. These microclusters exclude CD45 and signal as they translocate through the dSMAC and pSMAC, but they can also signal when arrested by barriers to MHCp transport (Mossman et al., 2005). When these clusters reach the cSMAC, they undergo a dramatic change in that CD45 becomes intermixed with TCR again, signaling stops, and LBPA accumulates in the cSMAC. The presence of LBPA in the cSMAC suggests that the cSMAC sorts TCR into multivesicular bodies for degradation. A higher level of membrane dye fluorescence in the cSMAC region is consistent with irregular membrane topology in the cSMAC or with cytoplasmic vesicular structures in the TIRFM field, both of which could carry CD45 without size-based exclusion. We demonstrate that F-actin is important both for microcluster formation as previously shown (Campi et al., 2005) and also for translocation and signaling.

MHCp levels on APCs regulate cSMAC size and the extent of TCR downregulation and thus free TCR levels. Regardless of the amount of MHCp encountered by T cells on APCs, signaling is sustained via formation of microclusters 11–17 TCRs in size. Thymocytes, which are ~10-fold more sensitive than T cells, do not form translocating TCR microclusters, and this absence of downregulation may result in more signal per agonist MHCp and greater sensitivity (Hailman et al., 2002).

In this microcluster-based model, high sensitivity to antigen can be achieved in one of at least two ways. Davis and colleagues have demonstrated that dimers of agonist MHCp paired with a self-MHCp can activate T cells outside of an IS (Krogsgaard et al., 2005). Self-MHCp also synergize with agonist MHCp in bilayer system experiments (Wülfing et al., 2002). However, when we dilute agonist MHCp to a few molecules per contact area with no addition of self-MHCp, we still get highly sensitive T cell activation (data not shown). This suggests that strong agonists like I-E^k-MCC88-103 for AND TCR nucleate TCR microclusters without dimer formation. Mechanisms by which single membrane bound ligands could trigger signaling have been proposed that involve CD45 (Choudhuri et al., 2005). CD45 is a pivotal phosphatase in TCR signaling that has an essential role in priming of Lck for activation (Koretzky et al., 1990), but can also act as a negative regulator of TCR signaling (D'Oro and Ashwell, 1999; Mustelin et al., 1995). The kinetic segregation model states that CD45 exclusion from sites of TCR engagement with agonist MHCp is a primary event in initiation of signaling and could allow a single TCR-MHCp interaction of sufficient kinetic stability to initiate TCR signaling (Choudhuri et al., 2005). We demonstrate here that microclusters formed by agonist MHCp engagement exclude CD45. This submicron exclusion zone may allow increased phosphorylation by tyrosine kinases in the cluster, including CD45-primed Lck that diffuses into the clusters from surrounding CD45-rich domains as recently demonstrated by single molecule imaging (Douglass and Vale, 2005). The subsequent colocalization of CD45 with the TCR in the cSMAC may contribute to inactivation of the kinase cascade as previously suggested (Freiberg et al., 2002). The mechanisms by which CD45 can be excluded from one site of TCR engagement, the microclusters, and accumulated in another, the cSMAC, is not known, but CD45 location appears to be controlled by both steric exclusion and lateral interactions (Choudhuri et al., 2005; Irles et al., 2003).

The first studies demonstrating small receptor clusters associated with signaling were performed with FcεRI engaged by multivalent ligands (Stauffer and Meyer, 1997; Wilson et al., 2000, 2001). Small FcεRI receptor clusters on mast cells are more efficient in signaling than larger clusters (Metzger et al., 1999), foreshadowing our finding that the large cSMAC is not a signaling structure. FcεRI and LAT clusters appear to undergo actin-dependent rearrangements on a relatively short length scale that leads to receptor endocytosis and termination of signaling (Wilson et al., 2000). Perhaps similar short-range mechanisms are invoked in regulation of TCR signaling in the case of anti-CD3-coated substrates in which cSMACs cannot form, yet T cells are effectively activated (Bunnell et al., 2001, 2002).

cSMAC formation is not required for T cell signaling (Lee et al., 2002, 2003). We now show that TCR-MHCp interactions in the cSMAC are not sufficient to sustain Ca^{2+} signaling. We have demonstrated this with an intervention that blocks formation of new microclusters while leaving the cSMAC intact. However, our finding that LBPA is specifically accumulated in the cSMAC directly supports the hypothesis that the cSMAC is involved in sorting of ubiquitinated TCR complexes for degradation as first proposed by Lee et al. (2002). We could not distinguish whether LBPA was recruited to the plasma membrane of the cSMAC and nearby endomembrane compartments versus only nearby endomembrane compartments by means of the standard LBPA staining conditions with detergent permeabilization. However, there are precedents for recruitment of the ESCRT complex to the plasma membrane (Lin et al., 2005). The mechanism by which Zap-70 is sometimes stably recruited to the cSMAC without evidence of function is not clear. Samelson and colleagues reported that initial recruitment of Zap-70-GFP to TCR clusters induced by anti-CD3 antibodies is dynamic but then evolves into a more stable interaction (Bunnell et al., 2002). However, there is no way to determine whether these dynamic and stable forms of Zap-70 function differently in the solid phase anti-CD3 system. One explanation for stably associated Zap-70 could be trapping in multivesicular body vesicles associated with the LBPA-positive cSMAC.

We conclude that the cSMAC is not involved in sustained Ca^{2+} signaling, but our observations on microclusters suggest that these structures rapidly acquire the chemical stability of the cSMAC, such that concepts originally applied to interactions in the cSMAC may be useful in understanding kinetics of interaction in microclusters (Lee et al., 2003).

Experimental Procedures

Materials

H57 (anti-TCRβ) and 14-4-4 (anti-I-E^k) hybridomas were obtained from ATCC, and D4 (anti-IE^k in complex with MCC) was a generous gift of M. Davis. Anti-CD45 I3/2.3 was obtained from T. Woodford-Thomas (Donald Danforth Plant Science Center, St. Louis, MO) (Trowbridge, 1978). Anti-lyso-bis-phosphatidic-acid (6C4) hybridoma supernatant was obtained from J. Gruenberg (University of Geneva) (Kobayashi et al., 1999). Biotinylated mouse isotype control was purchased from BD, Pharmingen. Latrunculin-A was purchased from Sigma. Agonist peptide MCC88-103 was from the Dana Farber Cancer Institute, Molecular Biology Core (Boston, MA). Alexa-fluor and other dyes were from Molecular Probes. Fab fragments were prepared by Papain digestion, purified by ion-exchange, and verified by SDS-PAGE. Fluorescent labeling of antibodies and Fab fragments was performed according to manufacturer's instructions.

Mice and Cell Culture

AND TCR transgenic mice were purchased from Jackson Laboratories (Bar Harbor, ME) and were crossed to B10.Br mice. All experiments were performed on F1 progenies between 8 and 12 weeks of age. AND T cells were activated in vitro as described (Campi et al., 2005). All mice were housed in specific pathogen-free conditions and cared for in accordance with protocol approved by Institutional and Animal Care and Use Committee.

Bilayers

Glass-supported DOPC bilayers incorporating GPI-anchored forms of I-E^k and ICAM-1 were prepared in flow cells (Bioptechs, Butler, PA) as described before (Grakoui et al., 1999). The bilayers were loaded with 50 μM MCC88-103 peptide in citrate buffer (pH 4.5) for 24 hr. The peptide loading efficiency was determined as described before and was 20%–30%. The type of fluorescent tagging of the proteins incorporated in the bilayer for different experiments are indicated in the figure legends. Unless otherwise specified, all the density of the proteins in the bilayers was: I-E^k 1-100 sites/μm^2 and ICAM-1 300 sites/μm^2.

Anti-LBPA Staining

Anti-LBPA staining was performed essentially as described (Kobayashi et al., 1999). AND T cells were made to interact with antigen-specific bilayers and after 30 min were fixed with 2% paraformaldehyde for 20 min. The cells were then incubated in media containing 50 mM NH_4Cl for 10 min. The cells were then blocked with 0.1% BSA for 20 min and then stained with the primary antibody (6C4) or isotype control for 30 min. The staining buffer contained 0.05% Saponin. This was followed by staining with a secondary antibody (anti-mouse IgG Fab_2).

Calcium Measurements

Intracellular calcium concentrations were measured by Fura-2 ratio. AND T cells were labeled with 2 μM of Fura-2 in serum-free media for 30 min at room temperature. The dye was washed with serum-containing media and further incubated at 37ºC for 30 min in serum-containing media. The cells were immediately used for experimentation after that. Images were acquired through a 40× NA 1.3 NeoFluar objective. The ratio of emission at 510 nm excited at 340 nm and 380 nm was determined with appropriate background subtractions. At the end of each experiment, high Ca^{2+} (1 μM ionomycin + 2 mM Ca^{2+} in media) and low Ca^{2+} (1 μM ionomycin + 0 mM Ca^{2+}, 2 mM EGTA in the media) were determined.

Microscopy

All microscopy was performed on an Olympus inverted IX-70 microscope equipped with a Xenon-arc lamp as light source, Ludl shutter and filter wheels equipped with appropriate excitation and emission filters, Ludl XY motorized state, piezo-electric stage for z movement of objective, Hamamatsu 12-bit ORCA-ER cooled CCD, Olympus TIRF module, and 2W Kr-Ar laser (Spectra Physics) launched in a single mode fiber (Oz Optics) via an AOTF (Solamere Technologies). The 60× 1.45 N.A. TIRF objective from Olympus was used for all experiments except for Fura-2 ratio imaging. The hardware on the microscope was controlled by IPLAB software on a Powermac G4 Macintosh computer.

TIRF Imaging of TCR

TIRF illumination was aligned according to manufacturer's instructions and was verified by making sure that fluorescence could be collected only from the bilayer plane. Reference particles that were more than 0.2 μm above the bilayer were not detected. Exposure times of 1–2 s were used to acquire images with 0.1 or 0.2 μm per pixel by the 60× 1.45 N.A. objective. For tracking purposes, images were collected at an interval of 6 s. Labeled anti-TCR Fab was present at 10 μg/ml throughout the experiment. Alexa488-conjugated

anti-human CD2 Fab at 10 μg/ml was used a control (Figure S1). We could not detect any signal from this Fab in the IS.

ZAP-70-GFP Transduction and Confocal Microscopy

AND T cells were transduced with ZAP-70-GFP and confocal microscopy was performed as described (Yokosuka et al., 2005).

Image and Data Analysis

Data was analyzed with the Metamorph, IPLab (Scanalytics, Vienna, VA) and ImageJ Software. For calibration of TIRFM images, the average number of TCR on AND T cell blasts measured with H57 Ab is 42,000 per cell or 140 molecules/μm^2 (Campi et al., 2005), which we assume to be the average TCR density for the population of all T cells adhering to ICAM-1 containing bilayers. We then measured the average fluorescence intensity (U/μm^2) for at least 25 T cells adhering to ICAM-1 bilayers and divided this by 140 to obtain the calibration value (U/molecule). The cSMAC and clusters (area > 0.16 μm^2) were measured and local background was subtracted based on area of 5–10 pixels near the structure that did not include a TCR cluster. We assume that free TCR diffuse in and around the engaged receptors in the cSMAC and peripheral TCR clusters. Then, the integrated fluorescence units in relevant area are divided by the U/molecule calibration value to determine the number of TCR in the structure. The results were internally consistent in that at 20 agonist MHCp/μm^2, 95% of the TCR were recruited to the cSMAC region at 30 min and the range of values in the TIRFM field with this calibration factor was near 40,000 at this antigen dose. Therefore, the average values for the cSMAC were consistent with other observations and the peripheral TCR clusters were measured with the same calibration value. One caveat of this estimate is that the TIRFM illumination field is not flat, so variation across the field will lead to errors in the determination of the number of TCR in individual clusters. Therefore, some of the spread in the data points may be due to local variation in illumination, but enough points were measured in different experiments to obtain similar mean values between experiments.

Supplemental Data

Supplemental Data include seven figures and six movies and can be found with this article online at http://www.immunity.com/cgi/content/full/25/1/117/DC1/.

Acknowledgments

We thank M. Davis, J. Huppa, J. Gruenberg, and T. Woodford-Thomas for key reagents. We thank T. Cameron and T. Sims for advice. This work was supported by NIH grants AI43542 and AI44931. R.V. was supported by a Bernard Levine Fellowship. G.C. was supported by a graduate fellowship from Boehringer Ingelheim. M.L.D. was supported by the Irene Diamond Foundation. Parts of this work were supported by a Riken Institute Collaborative Research Award.

Received: October 3, 2005
Revised: January 4, 2006
Accepted: April 12, 2006
Published: July 25, 2006

References

Beeson, C., Rabinowitz, J., Tate, K., Gutgemann, I., Chien, Y.H., Jones, P.P., Davis, M.M., and McConnell, H.M. (1996). Early biochemical signals arise from low affinity TCR-ligand reactions at the cell-cell interface. J. Exp. Med. *184*, 777–782.

Bromley, S.K., Iaboni, A., Davis, S.J., Whitty, A., Green, J.M., Shaw, A.S., Weiss, A., and Dustin, M.L. (2001). The immunological synapse and CD28–CD80 interactions. Nat. Immunol. *2*, 1159–1166.

Brossard, C., Feuillet, V., Schmitt, A., Randriamampita, C., Romao, M., Raposo, G., and Trautmann, A. (2005). Multifocal structure of the T cell-dendritic cell synapse. Eur. J. Immunol. *35*, 1741–1753.

Bunnell, S.C., Kapoor, V., Trible, R.P., Zhang, W., and Samelson, L.E. (2001). Dynamic actin polymerization drives T cell receptor-induced spreading: a role for the signal transduction adaptor LAT. Immunity *14*, 315–329.

Bunnell, S.C., Hong, D.I., Kardon, J.R., Yamazaki, T., McGlade, C.J., Barr, V.A., and Samelson, L.E. (2002). T cell receptor ligation induces the formation of dynamically regulated signaling assemblies. J. Cell Biol. *158*, 1263–1275.

Campi, G., Varma, R., and Dustin, M.L. (2005). Actin and agonist MHC-peptide complex-dependent T cell receptor microclusters as scaffolds for signaling. J. Exp. Med. *202*, 1031–1036.

Choudhuri, K., Wiseman, D., Brown, M.H., Gould, K., and van der Merwe, P.A. (2005). T-cell receptor triggering is critically dependent on the dimensions of its peptide-MHC ligand. Nature *436*, 578–582.

Costello, P.S., Gallagher, M., and Cantrell, D.A. (2002). Sustained and dynamic inositol lipid metabolism inside and outside the immunological synapse. Nat. Immunol. *3*, 1082–1089.

D'Oro, U., and Ashwell, J.D. (1999). Cutting edge: the CD45 tyrosine phosphatase is an inhibitor of Lck activity in thymocytes. J. Immunol. *162*, 1879–1883.

Douglass, A.D., and Vale, R.D. (2005). Single-molecule microscopy reveals plasma membrane microdomains created by protein-protein networks that exclude or trap signaling molecules in T cells. Cell *121*, 937–950.

Dustin, M.L., and Colman, D.R. (2002). Neural and immunological synaptic relations. Science *298*, 785–789.

Ehrlich, L.I., Ebert, P.J., Krummel, M.F., Weiss, A., and Davis, M.M. (2002). Dynamics of p56lck translocation to the T cell immunological synapse following agonist and antagonist stimulation. Immunity *17*, 809–822.

Freiberg, B.A., Kupfer, H., Maslanik, W., Delli, J., Kappler, J., Zaller, D.M., and Kupfer, A. (2002). Staging and resetting T cell activation in SMACs. Nat. Immunol. *3*, 911–917.

Grakoui, A., Bromley, S.K., Sumen, C., Davis, M.M., Shaw, A.S., Allen, P.M., and Dustin, M.L. (1999). The immunological synapse: a molecular machine controlling T cell activation. Science *285*, 221–227.

Hailman, E., Burack, W.R., Shaw, A.S., Dustin, M.L., and Allen, P.M. (2002). Immature CD4(+)CD8(+) thymocytes form a multifocal immunological synapse with sustained tyrosine phosphorylation. Immunity *16*, 839–848.

Hashemi, B.B., Slattery, J.P., Holowka, D., and Baird, B. (1996). Sustained T cell receptor-mediated Ca2+ responses rely on dynamic engagement of receptors. J. Immunol. *156*, 3660–3667.

Huppa, J.B., Gleimer, M., Sumen, C., and Davis, M.M. (2003). Continuous T cell receptor signaling required for synapse maintenance and full effector potential. Nat. Immunol. *4*, 749–755.

Iezzi, G., Karjalainen, K., and Lanzavecchia, A. (1998). The duration of antigenic stimulation determines the fate of naive and effector T cells. Immunity *8*, 89–95.

Irles, C., Symons, A., Michel, F., Bakker, T.R., van der Merwe, P.A., and Acuto, O. (2003). CD45 ectodomain controls interaction with GEMs and Lck activity for optimal TCR signaling. Nat. Immunol. *4*, 189–197.

Irvine, D.J., Purbhoo, M.A., Krogsgaard, M., and Davis, M.M. (2002). Direct observation of ligand recognition by T cells. Nature *419*, 845–849.

Johnson, K.G., Bromley, S.K., Dustin, M.L., and Thomas, M.L. (2000). A supramolecular basis for CD45 tyrosine phosphatase regulation in sustained T cell activation. Proc. Natl. Acad. Sci. USA *97*, 10138–10143.

Kobayashi, T., Beuchat, M.H., Lindsay, M., Frias, S., Palmiter, R.D., Sakuraba, H., Parton, R.G., and Gruenberg, J. (1999). Late endosomal membranes rich in lysobisphosphatidic acid regulate cholesterol transport. Nat. Cell Biol. *1*, 113–118.

Koretzky, G.A., Picus, J., Thomas, M.L., and Weiss, A. (1990). Tyrosine phosphatase CD45 is essential for coupling T-cell antigen receptor to the phosphatidyl inositol pathway. Nature *346*, 66–68.

Krogsgaard, M., Prado, N., Adams, E.J., He, X.L., Chow, D.C., Wilson, D.B., Garcia, K.C., and Davis, M.M. (2003). Evidence that structural rearrangements and/or flexibility during TCR binding can contribute to T cell activation. Mol. Cell *12*, 1367–1378.

Krogsgaard, M., Li, Q.J., Sumen, C., Huppa, J.B., Huse, M., and Davis, M.M. (2005). Agonist/endogenous peptide-MHC heterodimers drive T cell activation and sensitivity. Nature *434*, 238–243.

Krummel, M.F., Sjaastad, M.D., Wulfing, C., and Davis, M.M. (2000). Differential clustering of CD4 and CD3zeta during T cell recognition. Science *289*, 1349–1352.

Lee, K.H., Holdorf, A.D., Dustin, M.L., Chan, A.C., Allen, P.M., and Shaw, A.S. (2002). T cell receptor signaling precedes immunological synapse formation. Science *295*, 1539–1542.

Lee, K.H., Dinner, A.R., Tu, C., Campi, G., Raychaudhuri, S., Varma, R., Sims, T.N., Burack, W.R., Wu, H., Wang, J., et al. (2003). The immunological synapse balances T cell receptor signaling and degradation. Science *302*, 1218–1222.

Leupin, O., Zaru, R., Laroche, T., Muller, S., and Valitutti, S. (2000). Exclusion of CD45 from the T-cell receptor signaling area in antigen-stimulated T lymphocytes. Curr. Biol. *10*, 277–280.

Lin, Y., Kimpler, L.A., Naismith, T.V., Lauer, J.M., and Hanson, P.I. (2005). Interaction of the mammalian endosomal sorting complex required for transport (ESCRT) III protein hSnf7–1 with itself, membranes, and the AAA+ ATPase SKD1. J. Biol. Chem. *280*, 12799–12809.

Liu, H., Rhodes, M., Wiest, D.L., and Vignali, D.A. (2000). On the dynamics of TCR:CD3 complex cell surface expression and downmodulation. Immunity *13*, 665–675.

Malherbe, L., Hausl, C., Teyton, L., and McHeyzer-Williams, M.G. (2004). Clonal selection of helper T cells is determined by an affinity threshold with no further skewing of TCR binding properties. Immunity *21*, 669–679.

Matsuo, H., Chevallier, J., Mayran, N., Le Blanc, I., Ferguson, C., Faure, J., Blanc, N.S., Matile, S., Dubochet, J., Sadoul, R., et al. (2004). Role of LBPA and Alix in multivesicular liposome formation and endosome organization. Science *303*, 531–534.

Metzger, H., Chen, H., Goldstein, B., Haleem-Smith, H., Inman, J.K., Peirce, M., Torigoe, C., Vonakis, B., and Wofsy, C. (1999). A quantitative approach to signal transduction. Immunol. Lett. *68*, 53–57.

Mobius, W., van Donselaar, E., Ohno-Iwashita, Y., Shimada, Y., Heijnen, H.F., Slot, J.W., and Geuze, H.J. (2003). Recycling compartments and the internal vesicles of multivesicular bodies harbor most of the cholesterol found in the endocytic pathway. Traffic *4*, 222–231.

Monks, C.R., Freiberg, B.A., Kupfer, H., Sciaky, N., and Kupfer, A. (1998). Three-dimensional segregation of supramolecular activation clusters in T cells. Nature *395*, 82–86.

Mossman, K.D., Campi, G., Groves, J.T., and Dustin, M.L. (2005). Altered TCR signaling from geometrically repatterned immunological synapses. Science *310*, 1191–1193.

Mustelin, T., Williams, S., Tailor, P., Couture, C., Zenner, G., Burn, P., Ashwell, J.D., and Altman, A. (1995). Regulation of the p70zap tyrosine protein kinase in T cells by the CD45 phosphotyrosine phosphatase. Eur. J. Immunol. *25*, 942–946.

Reay, P.A., Matsui, K., Haase, K., Wulfing, C., Chien, Y.H., and Davis, M.M. (2000). Determination of the relationship between T cell responsiveness and the number of MHC-peptide complexes using specific monoclonal antibodies. J. Immunol. *164*, 5626–5634.

Savage, P.A., and Davis, M.M. (2001). A kinetic window constricts the T cell receptor repertoire in the thymus. Immunity *14*, 243–252.

Schamel, W.W., Arechaga, I., Risueno, R.M., van Santen, H.M., Cabezas, P., Risco, C., Valpuesta, J.M., and Alarcon, B. (2005). Coexistence of multivalent and monovalent TCRs explains high sensitivity and wide range of response. J. Exp. Med. *202*, 493–503.

Shaw, A.S., and Dustin, M.L. (1997). Making the T cell receptor go the distance: a topological view of T cell activation. Immunity *6*, 361–369.

Shimizu, Y., van Seventer, G.A., Horgan, K.J., and Shaw, S. (1990). Roles of adhesion molecules in T-cell recognition: fundamental similarities between four integrins on resting human T cells (LFA-1, VLA-4, VLA-5, VLA-6) in expression, binding, and costimulation. Immunol. Rev. *114*, 109–143.

Sperling, A.I., Sedy, J.R., Manjunath, N., Kupfer, A., Ardman, B., and Burkhardt, J.K. (1998). TCR signaling induces selective exclusion of CD43 from the T cell-antigen-presenting cell contact site. J. Immunol. *161*, 6459–6462.

Springer, T.A. (1990). Adhesion receptors of the immune system. Nature *346*, 425–434.

Stauffer, T.P., and Meyer, T. (1997). Compartmentalized IgE receptor-mediated signal transduction in living cells. J. Cell Biol. *139*, 1447–1454.

Trowbridge, I.S. (1978). Interspecies spleen-myeloma hybrid producing monoclonal antibodies against mouse lymphocyte surface glycoprotein, T200. J. Exp. Med. *148*, 313–323.

Valitutti, S., Dessing, M., Aktories, K., Gallati, H., and Lanzavecchia, A. (1995). Sustained signaling leading to T cell activation results from prolonged T cell receptor occupancy. Role of T cell actin cytoskeleton. J. Exp. Med. *181*, 577–584.

Wilson, B.S., Pfeiffer, J.R., and Oliver, J.M. (2000). Observing FcepsilonRI signaling from the inside of the mast cell membrane. J. Cell Biol. *149*, 1131–1142.

Wilson, B.S., Pfeiffer, J.R., Surviladze, Z., Gaudet, E.A., and Oliver, J.M. (2001). High resolution mapping of mast cell membranes reveals primary and secondary domains of Fc(epsilon)RI and LAT. J. Cell Biol. *154*, 645–658.

Wülfing, C., Sumen, C., Sjaastad, M.D., Wu, L.C., Dustin, M.L., and Davis, M.M. (2002). Costimulation and endogenous MHC ligands contribute to T cell recognition. Nat. Immunol. *3*, 42–47.

Yokosuka, T., Sakata-Sogawa, K., Kobayashi, W., Hiroshima, M., Hashimoto-Tane, A., Tokunaga, M., Dustin, M.L., and Saito, T. (2005). Newly generated T cell receptor microclusters initiate and sustain T cell activation by recruitment of Zap70 and SLP-76. Nat. Immunol. *6*, 1253–1262.

Zaru, R., Cameron, T.O., Stern, L.J., Muller, S., and Valitutti, S. (2002). Cutting edge: TCR engagement and triggering in the absence of large-scale molecular segregation at the T cell-APC contact site. J. Immunol. *168*, 4287–4291.